Combined radar monitoring of long surface waves packets in the Pacific Ocean

S. A. Velichko*, A. Ya. Matveev, D. M. Bychkov, V. K. Ivanov, V. N. Tsymbal

O. Ya. Usikov Institute for Radiophysics and Electronics of the National Academy of Sciences of Ukraine, 12, Acad. Proskura St., Kharkov, 61085, Ukraine

In order to continue and more detailed study of the manifestations of seismic activity on the World Ocean surface, in this work we verified the complex technique of airborne radar monitoring and research of long surface wave packets in the seismically active region in the Northwest Pacific Ocean near the Kuril-Kamchatka Trench.

When verifying the technique proposed in the previous work, we used data from two series of radar surveys of the sea surface within the study area in the 3-*cm* range of radio wave lengths. The first series of radar surveys had included tacks of flights along the north–south direction, to which, for comparison, the results of the second series in the west–east direction were added. These radar images, presented in the work, detect manifestations of two surface wave packets propagating from the same area, in the same direction, with an interval of 16 hours.

For a comprehensive study of surface wave packets based on a set of radar images of two series and to establish the nature of their origin, a combined spatial and spectral analysis of the nonlinear form of the wave packet components was performed. As a result, the spatial scale of surface wave packets (5–10 *km*), the lengths of the wave components of the packets (1–5 *km*) and the speed of packets movement (6.1 *m/s*) were determined. The analysis involved the parameters of the ocean-atmosphere near-surface layer, provided by operational *in situ* measurements, which were obtained by the research vessel "Akademik Petrov". This included the direction and speed of the near-surface wind, the state of wind waves and swell, the speed of the surface current, etc. In addition, data on bathymetry along the path of the surface wave packet and seismic activity in the area were used.

Finally, it was assumed that the observed packets of surface waves are Korteweg – de Vries solitons, which arise as a result of collapses on the steep underwater slopes of the Kuril-Kamchatka Trench due to a seismic shock and the aftershock that followed it. The developed airborne radar technique can also be used in satellite monitoring of the surface of the World Ocean in systems for warning about the approach of potentially dangerous long waves to the coast.

Keywords: airborne radar technique, surface wave packet, seismic collapse, soliton.

1. Introduction

Due to the impact of global warming on the World Ocean, both cyclonic activity and seismic activity along its perimeter have sharply increased. This leads to a growth in the number of powerful cyclones and hurricanes above the water surface, and the formation of disturbances on the surface that are dangerous for human activity, such as large wind waves, tsunamis, single and solitary waves. At present, to organize measures to prevent their consequences, radar information obtained with the help of constantly modernized radar methods is most efficiently and efficiently used.

In (Velichko et al, 2021), a complex experimental method was described for detecting manifestations of long surface wave (SW) packets in the open ocean, based on the results of radar monitoring. In the work, the processing and analysis of the received radar images (RI) were performed involving the real-time data of *in situ* measurements provided by the research vessel (R/V) "Akademik Petrov". The analysis also used data from the catalog of earthquakes in Kamchatka and the Commander Islands (Earthquakes Catalogue for Kamchatka, 2020) and bathymetric data from the NOAA National Centers for Environmental Information (NOAA National Centers, 2020). To verify the described method, in this paper, an extended analysis of the results of the previous study was performed with the involvement of additional research data. Recall that the surveys of the surface were carried out by an airborne (IL-18D, Fig. 1b, point 4) side-looking real aperture radar operating in the 3-*cm* radio wavelength range (SLRAR) "Analog" (Boev et al., 2007). The R/V "Akademik Petrov" (Fig. 1 b, point 5) was located in the experimental area, providing operational contact data on the state of the ocean-atmosphere near-surface layer, including wind speed and direction, wind wave and swell parameters, surface temperature, etc. For experiments, an area was selected in the northwestern part of the Pacific Ocean, approximately 300 *km* east of the city of Petropavlovsk-Kamchatsky (Fig. 1 b, point 5). The choice of the region was determined by its high seismicity. It contains the junction of four tectonic plates constantly shifting at a subduction rate of 2–9 *cm/year*: the Pacific, North American, Eurasian and Okhotsk (Fig. 1 a). In addition, along the eastern underwater slopes of the Kuril Islands

_____
E-mail: sergey19118@gmail.com

and to the southern part of the Kamchatka Peninsula, there is a narrow deep-water topographic depression: the Kuril-Kamchatka Trench. Its length is 2170 *km*, the average width is 59 *km*, and the maximum depth is 9717 *m* (Gnibidenko et al., 1980). On its steep slopes (about 7°), there are numerous ledges, terraces, as well as valleys descending to the maximum depth. The movement of tectonic plates (Fig. 1 a, points 1…3) can cause collapses and landslides in the trench and their manifestations on the sea surface.

For an extended analysis, the results of a radar search for the manifestations of SW, carried out during two series of flights with a difference of 16 hours, were used. At first, the monitoring was conducted by tacks in the direction north–south until the detection of the manifestations of SW on the last tacks of the flight (Fig. 2 a). At the beginning of the second series of flights in the west–east direction, the second packet of SW was found (Fig. 2 b). The analysis of the radar image series realized in the north–south direction was described in (Velichko et al, 2021). In this work, to increase the reliability of the analysis and its conclusions, the combined processing of radar images of two packages was carried out involving the contact data of the R/V "Akademik Petrov" and data from oceanographic studies.
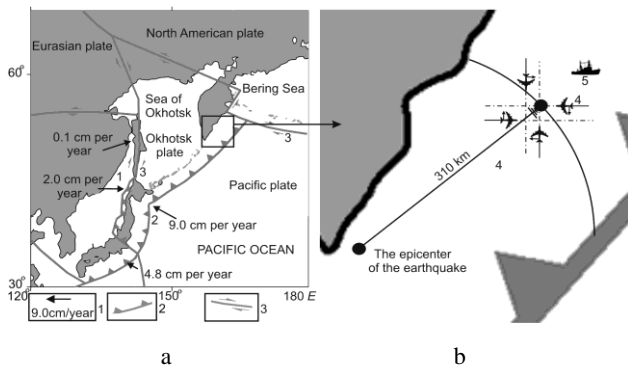

Fig. 1. Map of the experiment area:
a – Kuril-Kamchatka region and seismic activity zones;
b – enlarged map fragment of the observation site;
1, 2, 3 – speeds and directions of tectonic plates displacement;
4 – airborne radar surveys of wave packets;
5 – R/V "Akademik Petrov"

2. Combined processing and analysis of radar images of surface wave packets

Fig. 1 shows the area and routes of two flights of radar surveys of the sea surface, and Fig. 2 presents the radar images of the first and second series of flights, respectively. The wave packets were registered in the same area with a time difference of about 16 hours and the directions of their movement coincided. It can also be noted that if in the first series the SW packet was stably observed on the radar images of all tacks, then in the second series the SW packet begins to fade already on the radar image of the third tack. A possible reason for such an event is the weaker aftershock that followed the main seismic shock (Earthquakes Catalogue for Kamchatka, 2020) in the subduction zone (Fig. 1 a), which provoked the continuation of the rock collapse in the Kuril-Kamchatka Trench.
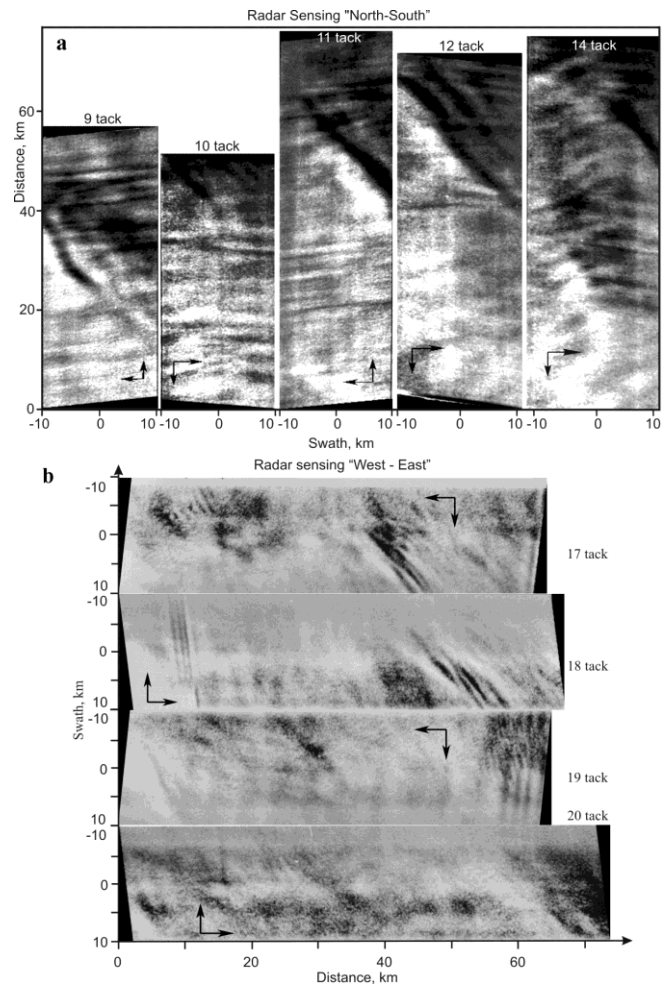

Fig. 2. Radar tacks: **a** – "North–South" (the first series); **b** – "West–East" (the second series).
|Arrows indicate the directions of the aircraft flight and radar scanning

An analysis of the first SW packet characteristics, carried out in (Velichko et al, 2021), showed that at the measured packet speed of 6.1 *m/s*, the real speed of its propagation would be about 7 *m/s*, taking into account the 1–1.5 *m/s* current from the North along the Eastern coast of the Kamchatka Peninsula. These current and weather conditions, according to the R/V "Akademik Petrov" data, did not change during the day of radio surveys. Therefore, it can be assumed that during the radar surveys of the second series, the conditions for the propagation of SW packets do not change, and the cause of its appearance may be the above-mentioned aftershock.

For the final conclusions about the origin of the observed wave packets, let us estimate the speeds and directions of motion of the two series of wave packets. Also, we consider the time and place of detection of packets, and compare this with seismic data, as well as with bathymetry data in the observation area. The formulation of these conclusions, supplemented by an analysis of the spatial and spectral characteristics of wave packets, makes it possible to determine their types.

Estimates of the speed and direction of wave packets propagation.

According to previous studies, the interaction of short-wavelength sea ripples with long waves of seismic

origin (Matveyev et al., 2010) has the following nature. The forward and back slopes of a long wave affect the spectrum and radio contrast of short waves in different ways. On the forward slope, short waves are attenuated; on the back slope, they are amplified. This is due to the direction of the vertical velocity of the liquid in a long wave. On the forward slope, it is directed upwards to the fluid and "smooths out" short waves, which leads to a decrease in radio contrast. On the back slope, where the fluid velocity in the long wave is directed downward, the effect is reversed. Such a difference in radio contrasts makes it possible to determine the speed of a packet of large waves observed by the radar method, using the movement of the packet on successive radar images. This becomes possible by tracking the contrast boundary between the forward and back slopes of a given packet wave.

In the case of the presence of long internal or atmospheric-gravity waves, the intensity of the surface short-wave scattering ripples is modulated by a system of variable surface currents or variations in the speed of the near-surface wind. These effects also lead to the creation of radio contrasts on the radar image, which are sufficient to detect large wave packets.

Updated data for calculating the speed and direction of wave packets from the radar images of the first and second series are given in Table 1 and Table 2. Here are the tack courses ψ_k for the 1st and 2nd series, the start and end times $T_{k\,st}$ and $T_{k\,end}$ of the tacks, as well as the radar images processing data, where k denotes the tack number.

Note that during processing, the observation swaths were preliminarily aligned in the local ground-based coordinate system relative to the central line of the swath, which was common to all lines of the series. Therefore, the processing was carried out by linking the radar image to this line (Fig. 2) and interactively determining the position of the packet wave fronts for each tack. As a result, the relative coordinates b_{k0} of the position of the wave packets along the oY and oX axes were determined (shown in Fig. 3 a for the first series), the corresponding relative observation times Δt_{k0} (Fig. 3 b, shown for both series), and the azimuths ϕ_{fk} of the wave packets propagation directions were calculated.

Table 1. Calculation of the speed and direction of wave packet propagation according to the front boundary position of the packet first wave (series 1)

tack (radar image) number series 1 on 12.08.1988	№ (k)	09 (1)	10 (2)	11 (3)	12 (4)	14 (5)
tack course	ψ_k, deg	0	180	0	180	180
start time	$T_{k\,st}$, GMT	3:46	4:00	4:18	4:31	5:05
end time	$T_{k\,end}$, GMT	3:54	4:08	4:26	4:39	5:13
front boundary coordinates, in oY	b_{k0}, km	23.30	42.50	58.40	63.80	69.83
relative time of the front boundary observation	Δt_{k0}, min	29.0	42.5	64	70	104
azimuth of wave packets propagation	ϕ_{fk}, deg	52.1	53.3	52.3	54.6	47.4

Table 2. Calculation of the speed and direction of wave packet propagation according to the front boundary position of the packet first wave (series 2)

tack (radar image) number series 2 on 12.08.1988	№ (k)	17 (1)	18 (2)	19 (3)	20 (4)
tack course	ψ_k, deg	270	90	270	90
start time	T_{k_st}, GMT	19:56	20:11	20:29	20:45
end time	$T_{k\,end}$, GMT	20:03	20:20	20:38	20:53
front boundary coordinates, in oX	b_{k0}, km	42.01	52.80	–	65
relative time of the front boundary observation	Δt_{k0}, min	78.9	97.3	–	131.7
azimuth of wave packets propagation	ϕ_{fk}, deg	54.1	47.9	–	48.9

The average geographic azimuths of the front propagation directions were $\overline{\phi}_{fk}^{(I)} = 51.9^*$ for the first series of observations and $\overline{\phi}_{fk}^{(II)} = 50.3^*$ for the second series. Based on these data, the propagation speeds of the 1st and 2nd wave packets were calculated. The speeds $V_{f0}^{(I,II)}$ were calculated from the shift of the packets centers in time along the flight line, with subsequent projection onto the normal to the packet front $V_{fn}^{(I,II)} = V_{f0}^{(I,II)} \cos\left(\overline{\phi}_f^{(I,II)}\right)$. Values of $V_{fn}^{(I)} = 6.2$ m/s for the first packet and $V_{fn}^{(II)} = 5.8$ m/s for the second packet were obtained, while the measurement errors are estimated within 10%.

Taking into account the place and time of the SW packets observation, as well as the direction (azimuth) and speed of propagation of the wave front boundary calculated from the series of radar images, the location of the supposed source of perturbations was estimated. According to (Earthquakes Catalogue for Kamchatka, 2020), this place coincided with the earthquake that occurred on August 11, 1988 at $T_S = 12.02.40.0$ GMT. The earthquake epicenter coordinates were $C_S = (50,78°\ N;\ 157,92°\ E)$, depth $H_S = 40$ km, energy class $E_S = 10$.
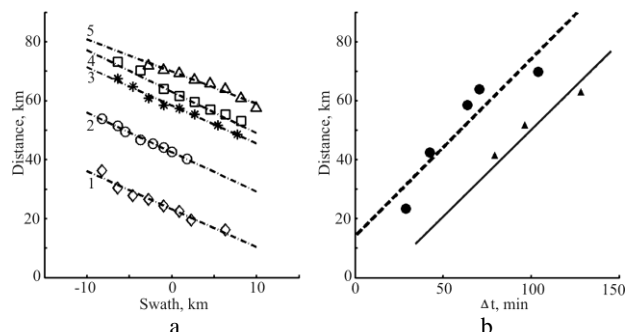

Fig. 3. a – the position of the boundary of the first wave front of the packet in local coordinates according to the 1st series of radar images data; b – dependence of the wave packets center position on the local observation time, according to the radar data of the first (circles ●) and second (triangles ▲) flight series. Here (dashed - -) and (solid -) are the regression lines of the packet motion equations

The direction azimuth from the point of the seismic shock to the region of radar observations of the SW packets is equal to $\varphi_S = 59^* \pm 2^*$. This is close to the azimuths of the direction of the wave packets propagation, taking into account the measurement accuracy of the latter.

The locations of the earthquake epicenter and the area of the surface wave packets observation are marked in Fig. 1 b. The coincidence of the epicenter position with the supposed source of the 2nd wave packet, observed by the 2nd series of surveys, can be explained by the aftershock. Such an aftershock could disturb the non-stationary equilibrium of the rock on the trench slope, which occurred in this place after the main seismic shock. This assumption is correlated with the data of the NOAA National Environmental Information Centers (NOAA National Centers, 2020) on the change in the bottom topography in the area of the presumed source of surface disturbance (Fig. 4). As can be seen, the bottom on the SW propagation path sharply changes its depth and there are ledges 20–30 *km* long, which can also affect the speed of SW packets propagation.
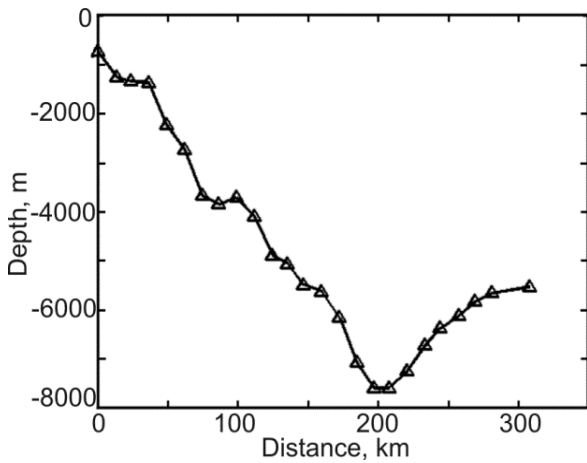

Fig. 4. Ocean floor profile from the seismic shock point to the SW packets observation point

To determine the type of observed wave packets, we analyze their spatial and spectral characteristics.

Spatial characteristics of SW packets in the areas of their observation were analyzed in sections along their direction of motion, after calibration with respect to scattering from the undisturbed sea surface. Fig. 5 shows the representative sections of the wave packets radar contrasts of the first and second series of flights.
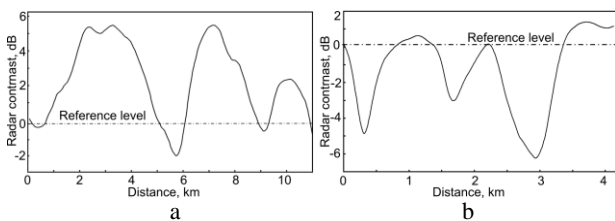

Fig. 5. a – calibrated cross-sections of wave packets radar contrast along their direction of motion, typical for radar images of the 1st series; b – 2nd flight series.
The line –.–.– denotes the reference level of radar contrast corresponding to the average scattering from the sea surface outside the zone of the SW packet presence

As can be noticed in Fig. 5, the waves observed in the packets have a non-linear shape, and their lengths are 3.6 *km*, 4.3 *km*, 4.9 *km*, 6.9 *km* for the first series of radar images (Fig. 5 a) and 1.1 *km*, 1.24 *km*, 1.4 *km*, 1.5 *km* for the second (Fig. 5 b). At the same time, the distance between the waves in the packet is not constant, and at the end of the second series, partial destruction of the SW packet was observed (Fig. 2).

To estimate the spectral characteristics of wave packets, the following factors are taken into account, which affect the accuracy of the determination. Namely, geometric and radiometric corrections were performed for the original radar images.

The geometric correction consisted in linking the radar images to a linear equal-scale horizontal projection on the underlying surface, which assumed:

• radar image transformation from coordinates "slant range – survey time" into linear coordinates on a horizontal surface. In this case, it is necessary to take into account the location of resolution elements on the surface depending on the scan angle and the speed of the carrier.

• equalization of spatial resolution across the swath, which depends on slant range, and along the swath, which depends on flight speed.

The transformations include the necessary filtering, as a result of which the size of the final resolution element was 100×100 *m²*.

The radiometric correction of the radar images consisted in adjustment of the average level of the radar scatter recording across the swath. The received radar signal can vary within 40 dB in power, which is due not only to a change in the slant range, but also to a variation in the scattering intensity from the angle of incidence on the sea surface. The angles of incidence in our case change from $\theta_{min} = 20^o$ at the beginning of the swath to $\theta_{max} = 80^o$ at the end of the swath. In addition, let us remind that in this instance, the radar image is the result of scattering by resonant ripples with wavelength $\lambda_S = \dfrac{\lambda_E}{2 \sin \theta}$, where λ_E is the electromagnetic wave length, so the scale λ_S differs across the swath. Consequently, the spatial spectrum will be correctly determined by the sections along the radar image swath, at a constant angle θ and a constant effective gain. Note that in this case, the spatial spectral components of large waves are initially calculated in projection on $\overline{\varphi}_f$ – the average azimuth of wave packet propagation.

To conduct spectral analysis of SW packets, a comparison of the average values and dispersion of scattering on the radar image sections of the "undisturbed surface" was carried out for different incident angles. The comparison showed that the random process of sea surface waves within these areas can be considered stationary, which made it possible to use the methods of standard statistical processing of random processes for quantitative estimates (Otnes et al., 1978). The power spectral density *Sxx* (PSD) was estimated using the fast Fourier transform (FFT) method. When calculating the PSD, frequency averaging was carried out by averaging five neighboring realizations by a sliding window and averaging over the ensemble.
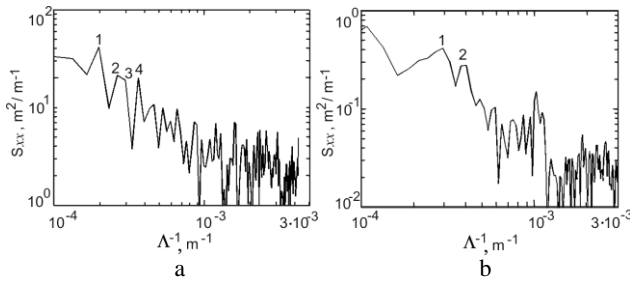
Fig. 6. a – power spectral density *Sxx* in sections along the direction of wave packets propagation on radar images of the first series; b – 2nd flight series

An analysis of the PSD *Sxx* (Fig. 6) shows that the largest peaks in the spatial frequency spectrum for the radar images of the first series correspond to surface wave lengths $\Lambda_1 = 5060$ *m*, $\Lambda_{2-3} = 3800$–3370 *m*, $\Lambda_4 = 2750$ *m*, and local maxima in the spectrum are observed down to values of the order of $\Lambda = 1000$ *m*.

For the radar images of the second series, typical spectrum wavelengths are $\Lambda_1 = 2200$ *m*, $\Lambda_2 = 1600$ *m*. At the same time, there is also a set of smaller spectral peaks in the range of 1500–1000 *m*.

Primary conclusions about the seismic nature of the origin of heterogeneities observed on the surface were described above. The final conclusion about the type of experimentally observed packets of nonlinear waves can only be given by their comparative analysis with long waves existing on the ocean surface.

3. Determining the type of experimentally observed nonlinear wave packets

Recall that we observe on each radar image a packet of two to three nonlinear waves, the distance between which changed from tack to tack. Therewith, at the end of the second series, a partial destruction of the wave packet takes place.

Let us consider different versions of the nature of the surface wave packets studied in our experiment. As the main criterion for comparison, we take the propagation speeds of waves of different origin, in the course of their effect on the ocean surface. The limitation only to this criterion is explained by the fact that the manifestation of large waves on the surface is approximately the same, in terms of the distribution of radar contrasts during their observation. The latter refers to different types of waves, from atmospheric to surface gravity and internal waves of the ocean.

a) Manifestations of <u>atmospheric internal gravity waves</u> (AIGW) on the ocean surface have been repeatedly observed on radar images from space, provided both by real aperture side-looking radars (SLRAR) of the "Analogue" type (Kalmykov et al., 1985; Mitnik et al., 1990), and by synthetic aperture radars (Alpers et al., 1996). The mechanism of AIGW mapping on the radar images of ocean is well described, and their appearances are quite similar to the wave packet effects that we observed, especially in the 1st flight tacks series. However, it should be noted (Gossard et al., 1975; Veltishev et al., 2006; Gill, 1982) that: 1) AIGWs are basically formed behind the coastal heights or islands, i.e. it is mainly the leeward waves;

2) the number of cycles in the AIGW group amounts to several tens, while in the wave packets here it was no more than 4; 3) at last, the near-surface wind speed was 3–5 *m/s* in the area of experiments, whereas the propagation speed of detected wave packets was ~ 6–7 *m/s* (taking into account the counter current). The latter is 2 times higher than that of possible AIGWs.

b) <u>Surface gravity waves.</u> The phase velocity of such waves is $V_{ph} = \sqrt{\dfrac{g}{K_0}\tanh(K_0 h)}$, where K_0 is a wavenumber, and in our case the depth of the ocean is $h \approx 7000$ *m* in the region of experiments. For surface wave lengths, which were determined from spatial spectra (Fig. 6), the range of phase velocities are $V_{ph}^{(I)} = 88 - 65$ *m/s* for the first series and $V_{ph}^{(II)} = 60 - 50$ *m/s* for the second series. The group velocities of the studied wave packets in this approximation would be $V_{gr}^{(I)} = 37$ *m/s* and $V_{gr}^{(II)} = 26$ *m/s*, accordingly. It is obvious that the calculated group velocities are 5–10 times higher than the maximum propagation speeds of observed wave packets, and the latter cannot consist of surface gravity waves.

c) <u>Internal waves (IW)</u>. Packets of internal waves have also been detected experimentally in many cases as well, e.g. (Jackson et al., 2002; Apel et al., 1983; Dwi Susanto et al., 2005). Of interest in terms of comparison with our studies are airborne radar investigations of internal wave packets (Sabinin et al., 2007), which included the ocean surface observations near the coast of Kamchatka over great depths, and where the airborne X-band radar was used.

Here one can note that the characteristic features of the observed IW packets are 1) their generation mainly on the shelf or tidal currents, 2) their relatively low phase velocity. Typically, phase velocities less than 1 *m/s* were indicated, the maximum observed ones were up to 3 *m/s*, which is at least 2 times lower than the propagation speed of the packets we found.

d) <u>Solitons of surface waves.</u> Obviously, the observed wave packets are not a solitary wave (soliton), but it can be assumed that they are group solitons, or envelope solitons. This assumption may be supported by the fact that the propagation speeds of the latter are not directly related to the phase velocities of the component waves, e.g. (Filippov, 1990; Zeytounian, 1995). The argument against this assumption is that the number of harmonics inside a group soliton is usually 14 to 20, and not 3-4, as in our case.

e) As a result, it remains to be assumed that the observed wave packet is a Korteweg – de Vries (KdV) soliton (Korteweg & deVries, 1895; Zeytounian, 1995), and its formation may be associated with a collapse on the slope of the Kurilo-Kamchatsky Trench (Fig. 4) (Earthquakes Catalogue for Kamchatka, 2020) due to an earthquake. The form of the KdV soliton and its speed are determined by the conditions for compensating the effects of nonlinearity and dispersion. When the original soliton splits into several, all solitons move in the same direction with speeds proportional to their heights. In some cases, KdV solitons can be considered as particles obeying the laws of motion of Newtonian mechanics.

Even when passing through a small inhomogeneity of the medium, for example, a small local change in depth, the soliton not only slows down or speeds up, but also slightly deforms. However, having passed the obstacle, it restores its form and speed (Filippov, 1990). This behavior of KdV solitons on the sea surface is consistent with changes in the discrete waves observed in the packet during radar surveys at different tacks (Fig. 2 b). The appearance of a wave packet can also be explained by the frequently observed disintegration of a single soliton into several at the initial stage during the collapse. Their lower propagation speed, compared to gravitational waves, can be associated with their small amplitudes, which also agrees with our theoretical estimates (Boev, 2011). In this case, the average group velocity of solitons will be strongly influenced by the bottom topography along the path of their propagation (Fig. 4).

4. Conclusions

The paper presents the results of complex studies of large-scale wave packets on the ocean surface using the data of airborne X-band side-looking real aperture radar. In continuation to the first publication (Velichko et al., 2021), the results of processing radar image matrices (RI) for 2 series of aircraft experiments were used. The flight tacks of the 1st series were carried out along the meridional direction, the 2nd series – along the latitudinal direction. The observation area was the northwestern part of the Pacific Ocean, 300 *km* from the Kamchatka Peninsula, in the Kuril-Kamchatka zone of seismic activity.

Spatial and spatial-spectral processing of the RI series made it possible to establish that the propagation speeds and azimuths of the observed large-scale wave packets manifestations were $V_{fn}^{(I)} = 6.2$ *m/s* and $\overline{\varphi}_{fk}^{(I)}$ for the first series of observations, $V_{fn}^{(II)} = 5.8$ *m/s* and $\overline{\varphi}_{fk}^{(II)} = 50.3^*$ – for the second series, respectively. The wavelengths of the spatial components of the packets were estimated as 3.6–6.9 *km* for the first packet and 1.1–1.5 *km* for the second. The calculated main spectral components of the packets are 2750–5060 *m* and 1600–2200 *m*, with local extrema of the spectrum down to 1000 *m*.

Based on the data obtained, an analysis of the possible nature of the observed large wave packets manifestations on the ocean surface was carried out. Both meteorological data and bathymetry were taken into account. It is shown that the most probable reason for the formation of wave packets were rock falls in the Kuril–Kamchatka Trench, triggered by a seismic shock (series 1) and the subsequent aftershock (series 2). To analyze the type of wave packets, the speed of their propagation, determined from the series of radar images, was used.

Comparison with the phase velocities of long waves typical of the ocean made it possible to assume that the observed packets of nonlinear waves are Korteweg – de Vries (KdV) solitons (Korteweg & deVries, 1895; Zeytounian, 1995).

References

Alpers, W., Stilke, G. (1996). Observation of a nonlinear wave disturbance in the marine atmosphere by the synthetic aperture radar aboard the ERS-1 satellite. *J. Geophys. Res.*, 101(C3), 6513–6525.

Apel, J. R., & Holbrook, J. R. (1983). Internal solitary waves in the Sulu Sea. *Johns Hopkins APL Technical Digest,* 4(4), 267–275.

Boev, A. G., Boeva, A. A., Matveyev, O. Y. (2010). Radar contrast of wind ripples on the sea wave of seismic origin. *Radio Physics and Radio Astronomy*, 15(4), 453–461. DOI: https://doi.org/10.15407/rpra.

Boev, A. G., Efimov, V. B., Tsymbal, V. N. (Ed.), Yatsevich, S. Ye., Kalmykov, I. A., Kurekin, A. S., … Dranovskii, V. I. (Eds.) (2007). *Radar methods and facilities for operational Earth remote sensing from airborne and spaceborne carriers.* Kiev : NAS of Ukraine Publ.

Dwi Susanto, R., Mitnik, L., Zheng, Q. (2005). Ocean internal waves observed in the Lombok Strait, *Oceanography*, 18(4), 80–87.

Earthquakes Catalogue for Kamchatka and the Commander Islands (1962 – present). (2020). Retrieved from http://sdis.emsd.ru/info/earthquakes/catalogue.php?out=info.

Filippov, A. T. (1990). *Diversiform soliton*. 2nd Ed. Moscow : Nauka Publ.

Gill, A. E. (1982). *Atmosphere-Ocean Dynamics*. (Vol. 1). New York : Academic Press Publ.

Gnibidenko, G. S., Bykova, T. G., Veselov, O. V., Sychev, P. M. (Eds.) (1980). *Tectonics of Kuril-Kamchatka Trench.* Moscow : Nauka Publ.

Gossard, E. E., Hooke, W. H. *Waves in the atmosphere*. Elsevier Scientific Publishing, 1975.

Jackson, R. C., Apel, J. R. (2002). *An Atlas of Oceanic Internal Solitary Waves by Global Ocean Associates. Oceanic Internal Waves and Solitons*. Retrieved from http://www.internalwaveatlas.com/Atlas_index.html.

Kalmykov, A. I., Nazirov, M., Nikitin, P. A., Spiridonov, Yu. G. (1985). On ordered mesoscale structures on the ocean surface, revealed from data of radar observation from space. *Issled. Zemli iz Kosmosa*, 3, 41–47.

Korteweg, D. J., de Vries, G. (1895). On the Change of Form of Long Waves Advancing in a Rectangular Canal, and on a New Type of Long Stationary Waves. *Phil. Mag.* Ser. 5, Vol. 39, No. 240, 422–443.

Matveyev, O. Y., Boev, A. G., Boeva, A. A. (2010, November). Radar contrast of wind ripples on the seismic origin wave. Proc. of 8th All-Russian Open Annual Conference Modern problems of Remote sensing of the Earth from Space, Moscow: IKI RAN, 217.

Mitnik, L. M, Viktorov, S. V. (Eds.) (1990). *Radar sensing of Earth surface from space.* Leningrad : Gidrometeoizdat Publ.

NOAA National Centers for Environmental Information. Bathymetric Data Viewer. (2020). Retrieved from https://www.ncei.noaa.gov/maps/bathymetry/.

Otnes, R. K., Enochson, L. (1978). *Applied Time Series Analysis. Basic Technologies*. (Vol. 1). New York : Willey Publ.

Sabinin, K. D., Serebryanyi, A. N. (2007). "Hot Spots" in the Field of Internal Waves in the Ocean. *Acoustics J.,* 53(3), 410–436.

Velichko, S. A., Matveev, A. Ya., Bychkov, D. M., Ivanov, V. K., Tsymbal, V. N., & Gavrilenko, O. S. (2021). Radar monitoring of long surface waves in the Pacific Ocean. *Radiofiz. elektron.* 26(1), 3–11. DOI: https://doi.org/10.15407/rej2021.01.

Veltishev, N. F., Stepanenko, V. M. (2006). *Mesometeorological processes*. Moscow : MSU Publ.

Zeytounian, R. Kh., (1995). Nonlinear long waves on water and solitons. *Phys. Usp.*, 38:12, 1333–1381. .

KОМПЛЕКСНИЙ РАДІОЛОКАЦІЙНИЙ МОНІТОРИНГ ПАКЕТІВ ДОВГИХ ПОВЕРХНЕВИХ ХВИЛЬ У ТИХОМУ ОКЕАНІ.

С. А. Величко, О. Я. Матвєєв, Д. М. Бичков, В. К. Іванов, В. М. Цимбал

Інститут радіофізики та електроніки ім. О. Я. Усикова НАН України, вул. Акад. Проскури, 12, Харків, 61085, Україна

З метою продовження та більш детального вивчення проявів сейсмічної активності на поверхні Світового океану в цій роботі верифіковано комплексну методику авіаційного радіолокаційного моніторингу та досліджено пакети довгих поверхневих хвиль у сейсмічно активному районі у північно-західній частині Тихого океану поблизу Курило-Камчатського жолоба.

При верифікації методики, запропонованої в попередній роботі, використані дані серій радіолокаційних знімань морської поверхні досліджуваного району в 3-см діапазоні довжин радіохвиль у напрямку "північ-південь", до яких для порівняння додані результати знімань у напрямку "захід-схід". На радіолокаційних зображеннях, наведених у роботі, виявлено прояви двох пакетів хвиль, що рухаються з однієї ділянки поверхні в одному напрямку з інтервалом 16 годин.

Для комплексного дослідження пакетів поверхневих хвиль за сукупністю радіолокаційних зображень двох серій та встановлення природи їх походження було виконано спільний просторовий та спектральний аналіз нелінійної форми складових хвильових пакетів. У результаті визначено просторовий масштаб пакетів поверхневих хвиль (5–10 км), довжини хвильових складових пакетів (1–5 км) та швидкість їх переміщення (6,1 м/с). До аналізу залучалися оперативні контактні дані про стан приповерхневого шару океан–атмосфера, отримані за допомогою науково-дослідного судна "Академік Петров", що включають напрямок та швидкість приповерхневого вітру, стан вітрового хвилювання та брижів, швидкість поверхневої течії та ін. Крім того, використані дані про батиметрію по трасі руху пакета поверхневих хвиль та сейсмічної активності в цьому районі.

Зроблено припущення, що пакети поверхневих хвиль, які спостерігаються, є солітонами Кортевега – де Фріза, що виникають внаслідок обвалів на крутих підводних схилах Курило-Камчатського жолоба через сейсмічний поштовх і афтершок, який стався після нього. Розроблена радіолокаційна авіаційна методика може бути використана під час супутникового моніторингу поверхні Світового океану в системах попередження про наближення потенційно небезпечних довгих хвиль до узбережжя.

Ключові слова: авіаційна методика радіолокації, пакет поверхневих хвиль, сейсмічний обвал, солітон.